

Article

Effect of Cryogenic Treatment on the Microstructure and Wear Resistance of 17Cr2Ni2MoVNb Carburizing Gear Steel

Yongming Yan ^{1,*}, Zixiang Luo ² , Ke Liu ³, Chen Zhang ³, Maoqiu Wang ¹ and Xinming Wang ²¹ Central Iron & Steel Research Institute Company Limited, Beijing 100081, China; maoqiuwang@hotmail.com² School of Material Science and Engineering, Xiangtan University, Xiangtan 411105, China; 201921001459@smail.xtu.edu.cn (Z.L.); wangxm@xtu.edu.cn (X.W.)³ Jianglu Machinery and Electronics Group Co., Ltd., Xiangtan 411100, China; liuke820x@126.com (K.L.); zc719500@163.com (C.Z.)

* Correspondence: yanyongming@necast.com; Tel.: +86-010-62182728

Abstract: Cryogenic treatment as a process that can effectively improve the performance of steel materials is widely used because of its simplicity and speed. This paper investigates the effects of different low temperature treatments on the microstructure and properties of 17Cr2Ni2MoVNb steel. The low temperature treatment range is divided into cryogenic treatment (CT-80), shallow cryogenic treatment (SCT-150) and deep cryogenic treatment (DCT-196), all with a duration of 1 h. The retained austenite content and the change in carbide volume fraction at 0.2 mm in the carburised layer are studied. The microhardness gradient of the carburised layer, as well as the friction coefficient and wear scar morphology at 0.2 mm, was investigated. The results show that the low temperature treatment is effective in reducing the retained austenite content and increasing the volume fraction of carbide. The lowest retained austenite content and highest carbide volume fraction were obtained for DCT-196 specimens at the same holding time. Due to the further transformation of martensite and the diffuse distribution of carbides, the microhardness and frictional wear properties of DCT-196 are optimal. Therefore, low temperature treatment can change the microstructure of the case layer of 17Cr2Ni2MoVNb steel and effectively improve the mechanical properties of materials.

Keywords: cryogenic treatment; 17Cr2Ni2MoVNb; wear; gear steel; carbide; retained austenite

Citation: Yan, Y.; Luo, Z.; Liu, K.; Zhang, C.; Wang, M.; Wang, X. Effect of Cryogenic Treatment on the Microstructure and Wear Resistance of 17Cr2Ni2MoVNb Carburizing Gear Steel. *Coatings* **2022**, *12*, 281. <https://doi.org/10.3390/coatings12020281>

Academic Editor: Alessio Lamperti

Received: 17 January 2022

Accepted: 14 February 2022

Published: 21 February 2022

Publisher's Note: MDPI stays neutral with regard to jurisdictional claims in published maps and institutional affiliations.



Copyright: © 2022 by the authors. Licensee MDPI, Basel, Switzerland. This article is an open access article distributed under the terms and conditions of the Creative Commons Attribution (CC BY) license (<https://creativecommons.org/licenses/by/4.0/>).

1. Introduction

The 17Cr2Ni2MoVNb steel developed from 18CrNiMo7-6 steel undergoes low distortion during carburizing heat treatment. The carburised layer presents a very complex microstructure due to the carbon concentration gradient distribution. It is composed of high carbon tempered martensite, retained austenite and carbides close to the surface, which provide high hardness and good wear resistance. The matrix is composed of low carbon tempered martensite, which supports sufficient toughness and strength. The 17Cr2Ni2MoVNb steel exhibits high strength, toughness, and fatigue properties, making it the potential material for high-strength carburizing steel. However, 17Cr2Ni2MoVNb steel contains a considerable amount of Ni, which enhances the stability of austenite. After carburizing, a substantial amount of carbon and alloying elements is dissolved in the matrix, which significantly reduces the start temperature of martensite transformation (M_s point). A large amount of austenite is retained in the carburized layer after carburizing and air cooling. Reheating and quenching cannot reduce the content of retained austenite, and the hardness cannot be further improved to meet the design requirements. In addition, the retained austenite is heated or transformed under strain during use, causing dimensional changes and redistribution of stress, which may also cause cracks during grinding and finishing. At present, the main ways to reduce the amount of retained austenite are high-temperature tempering and cryogenic treatment [1–4]. Cryogenic treatment has been widely used for tools, bearings, gears, and other workpieces made of high speed-steel, hard alloys and

other materials. As an example, the effect of cryogenic treatment on the wear resistance of 20CrNi2Mo steel was studied by Preciado and co-workers [5]. Their results showed that the wear resistance of the carburized sample was, respectively, improved by 17% and 25.5% after cryogenic treatment at -80 and -196 °C compared to conventional heat treatment.

Meanwhile, Kara's team has been systematically studying the application of deep cooling treatment to tools, tool steels and bearing steels [6–9]. Çiçek [6] found that cryogenic treatment with tempering treatment increases the average size of α -phase and forms η -phase in WC-CO tools, thus increasing the microhardness of the tools. Gunes [7] studied the wear behaviour of bearing steel AISI 52100 held at -145 °C for different times. It was shown that 36 h is the optimum holding time. At this holding time, the wear rate and friction coefficient decrease and the hardness reaches its maximum. Kara [8] applied cryogenic treatment to AISI D2 tool steel and ceramic tools. Artificial intelligence methods called artificial neural networks (ANNs) are used to estimate surface roughness based on cutting speed, cutting tool, workpiece, depth of cut, and feed rate. It was shown that the samples subjected to the DCTT-36 process gave the best results in terms of surface roughness and tool wear. The effect of cryogenic treatment on the surface roughness and wear of AB2010 tools was significantly improved. The highest micro and macro hardness values were obtained under the DCT-36 process. The secondary carbide formation of the samples was more uniform in the DCTT-36 process. Kara [9] used the L18 orthogonal experimental table to determine the best surface roughness (R_a) worth control factors for AISI 5140 steel. By using in the cylindrical grinding process of AISI 5140 steel and identified optimum grinding conditions via the Taguchi optimization method.

Current research on 17Cr2Ni2MoVNB steel has mainly focused on the study of the influence of process parameters such as the carburizing, quenching and tempering temperature on the structure and properties of the steel. The effect of the quenching temperature on the microstructure and rolling contact fatigue behaviour of 17Cr2Ni2MoVNB steel was investigated by Zhang and Qu [10,11]. The results showed that failure mode of the sample quenched at 900 °C is delamination, whereas the failure mode after quenching at 1100 °C is pitting corrosion. The effects of the tempering temperature on the tensile properties and rotary bending fatigue behaviour of this steel were also investigated, demonstrating that the tensile strength and fatigue strength were the highest at 180 °C, reaching 1456 and 730 MPa, respectively. At present, however, there are few reports on the effect of cryogenic treatment on the structure and mechanical properties of 17Cr2Ni2MoVNB steel after carburization. In this study, the changes in the microstructure and mechanical properties of 17Cr2Ni2MoVNB steel subjected to cryogenic treatment at three different temperatures are discussed and compared with those of the sample without cryogenic treatment.

2. Experiment

2.1. Materials and Heat Treatment

The experimental materials used in the present study were provided by the Central Iron and Steel Research Institute. The chemical composition of this steel was tabulated in Table 1.

Table 1. Chemical composition of 17Cr2Ni2MoVNB (wt.%).

C	Si	Mn	Cr	Ni	Mo	Nb	V	Fe
0.17	≤ 0.4	0.77	1.68	1.60	0.29	0.04	0.10	Bal.

Carburizing and tempering are important means of obtaining high hardness and high wear resistance on the surface while ensuring that the matrix has high toughness [12]. Therefore, all samples investigated in this work were first subjected to conventional heat treatment, followed by cryogenic treatment.

Conventional heat treatment consists of normalizing, thermal refining, carburizing, quenching in oil, and tempering. Round steel of diameter of 120 mm was forged into a ring

sample with an inner diameter of 70 mm, an outer diameter of 211 mm and a height of 40 mm. The ring samples were normalized, quenched, tempered, and then cut into samples of dimensions 20 mm × 20 mm × 20 mm. The cubic samples were prepared using the process shown in Figure 1. The continuous BH gas carburizing temperature was 930 °C and the total carburizing time was 10 h, then carburizing was followed by high-temperature tempering at 620 °C for 4 h. The samples were held at 800 °C for 1 h, then quenched in oil. After quenching, the low temperature tempering at 150 °C was carried out for 4 h. The samples were held at 800 °C for 1 h, then quenched in oil. After quenching, the low temperature tempering at 150 °C was carried out for 4 h. The carbon content of the sample from the matrix to the surface increased from 0.17% to approximately 1% after carburizing. The increased carbon content leads to the changes in the composition and microstructure of the carburized layer. Cryogenic treatment is employed to eliminate the retained austenite and improve the hardness and wear resistance of the carburized layer [12–16].

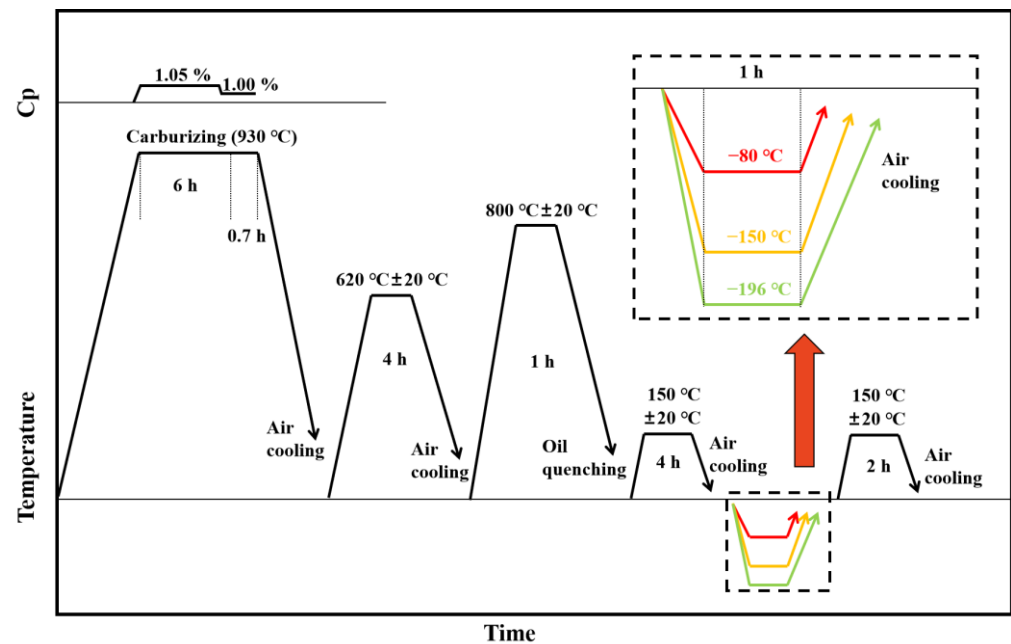


Figure 1. Schematic illustration of the carburizing and heat treatment processes of the experimental steel. Cp denotes the carbon potential during the carburizing process.

Liquid nitrogen was used as the cooling medium. The liquid nitrogen immersion method used in traditional cryogenic treatment easily leads to the formation of the cracks. Therefore, the equipment developed based on the aerosol method, (GL-150 cryogenic treatment experimental furnace produced by Shanghai GaoLe Machinery Equipment Co., Ltd. (Shanghai, China)) shown in Figure 2 was used to avoid the formation of the cracks. The samples for cryogenic treatment were suspended using a wire. The entire experiment was equipped with a real-time temperature sensor for temperature control. The three cryogenic treatment temperatures were designated as -80 , -150 and -196 °C as shown in Table 2, and the corresponding samples are denoted as CT-80, SCT-150 and DCT-196, respectively. After each cryogenic heat treatment process, the samples were subjected to low-temperature tempering at 150 °C for 2 h.

Table 2. Process name and description.

Process Name	Process Description
Conventional Heat Treatment (CHT)	-
Cryogenic treatment (CT-80)	Hold at -80 °C for 1 h
Shallow cryogenic treatment (SCT-150)	Hold at -150 °C for 1 h
Deep cryogenic treatment (DCT-196)	Hold at -196 °C for 1 h

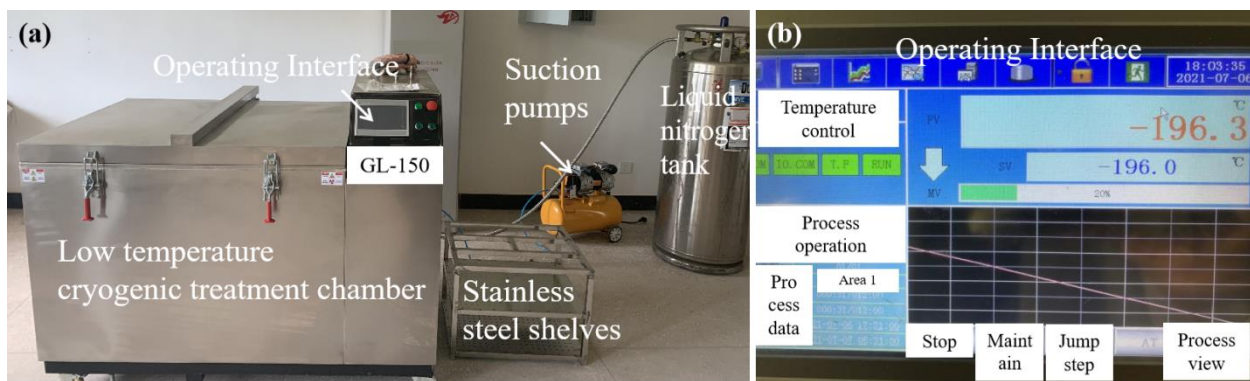


Figure 2. (a) Cryogenic treatment chamber, and (b) cryogenic treatment real time display interface.

2.2. Microstructural Characterization

The scanning technology can provide an important basis for explaining the influence of cryogenic treatment on the wear resistance of materials from the microstructure change [12,14,16]. The samples were cut into 10 mm × 10 mm × 10 mm cubes using an electric spark wire, and then polished with 400, 600 and 800 mesh sandpaper after inlay. Etching was performed using 4% nitric solution for a period of 10 s followed by rinsing with water and drying using a blower. The microstructures of the samples before and after cryogenic treatment were evaluated using a Zeiss EVO MA-10 metallographic microscope (Carl Zeiss, Jena, Germany), scanning electron microscope in bright field (SEM, Carl Zeiss, Jena, Germany)) and energy disperse spectroscopy (EDS, Carl Zeiss, Jena, Germany)).

The content of retained austenite affects the short fatigue crack growth, fatigue performance and wear resistance of carburized steel [5,12]. The content of retained austenite was determined using an X-ray diffractometer (Rigaku, D/MAX-2500/PC (Tokyo, Japan)) with a Cu X-rays source at a power of 18 kW, using a scanning speed for 1°/min. Data were acquired at diffraction angles of 40°–90°.

2.3. Microhardness and Wear Resistance Tests

The microhardness of all the specimens was measured using a Vickers hardness testing machine (HUAYIN, HVT-1000A, Laizhou Huayin, Laizhou, China) with a diamond indenter. The microhardness was measured according to Chinese National Standard GB/T9451-2005 “Determination and Calibration of the depth of the carburizing and quenching hardened layer of steel parts”. A load of 9.8 N was applied for a time-period of 10 s. To improve the accuracy, the hardness was determined at five distinct points in different regions of the specimen and the average value was taken. Friction and wear experiments were carried out using a CFT-1 comprehensive tester (Zhongke Kaihua, Lanzhou, China) to evaluate the material surface as shown for Figure 3. The wear mode was reciprocating, the friction surface of the sample was a carburized surface, and the dimensional area is 10 mm × 10 mm. The friction pair was Si₃N₄ ceramic balls, the friction conditions were: 20 °C, dry friction, load of 30 N, reciprocating speed of 500 times/minute, and reciprocating distance of 5 mm. The wear mark depth and wear volume were measured using a probe sensor, and tested after manual zero setting. The measurement method involved taking the upper, middle and lower three points of a wear mark, and the experimental data were acquired three times at one point.

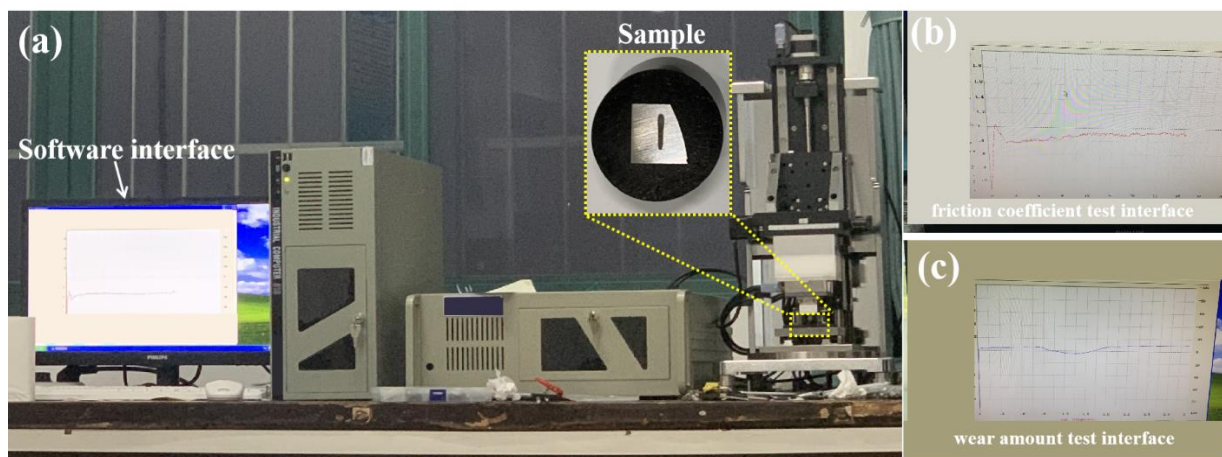


Figure 3. (a) CFT-1 comprehensive material surface property tester, (b) friction coefficient test interface, and (c) wear amount test interface.

3. Results and Discussion

3.1. Effect of Cryogenic Treatment on Microstructure

The changes in the microstructure including changes in the martensite structure, retained austenite and carbides after cryogenic treatment were investigated by SEM and X-ray Diffraction (XRD). Figure 4a,b shows the SEM images of the carburized layer at 0.2 mm from the surface in the four samples, indicating that the microstructure of the 17Cr2Ni2MoVNb steel is mainly composed of plate martensite (gray), retained austenite (concave) and finely dispersed precipitates of carbides (small white grains), the same as that of other carburized steels [5]. As shown in Figure 4a, the sample subjected to the CHT process contained a small amount of carbide precipitations, large areas of carbide accumulation were not detected. During the three cryogenic treatment processes, the amount of carbide precipitated along the grain boundary increased, and the carbide grew to form discontinuous networks, as shown in Figure 4b–d. An EDS point of the local enlargement of Figure 4d was performed to analyse the elemental composition of carbide and matrix, and the results are shown in Table 3. At least 10 regions were analysed for each specimen. The content of C and Cr elements at points P₁ and P₂ is higher than that in the matrix, thus it is speculated that Cr-rich carbide is present in the carburized layer.

The carbide content and the carbide distribution with relative frequency (the number of carbides per area) were correlated with the size of carbides 0.2 mm below the surface using the Image-Pro Plus software (version 6.0) [17]. The images were first processed with Photoshop (PS) to obtain Figure 4e–h and then processed with area statistics of Image-Pro. The calculated data is converted into μm units by scale. The obtained data were processed using origin software [17] using a built-in Gaussian function to fit the histogram data. The final volume fraction and carbide size distribution graph were obtained. The results are shown in Figure 4i–l. The calculated carbide content is 6.15%, 8.3%, 8.7% and 8.9% for the CHT, CT-80, SCT-150 and DCT-196 samples, respectively. The size of the majority of the carbides in the four samples was below 0.6 μm , whereas less carbides with a particle size of over 0.4 μm was detected. The relative frequency of the 0–0.2 μm carbides particles and 1.4–1.6 μm particles in DCT-196 was higher than that in the other samples. It can be seen that the number of carbides increased after cryogenic treatment. As the cryogenic treatment causes the lattice constant of iron to tend to contract, this increases the lattice distortion caused by supersaturated carbon atoms, which enhances the thermodynamic driving force for carbon atom precipitation. As a result, the solubility of carbon atoms decreases. In addition, the diffusion of carbons becomes more difficult at low temperatures and the diffusion distance becomes shorter. As a result, a large number of dispersed ultrafine carbides precipitate on the martensite. Huang and Kelkar used M2 steel as the

experimental object and concluded that cryogenic treatment promoted carbide precipitation and also contributed to a more diffuse carbide distribution [18,19].

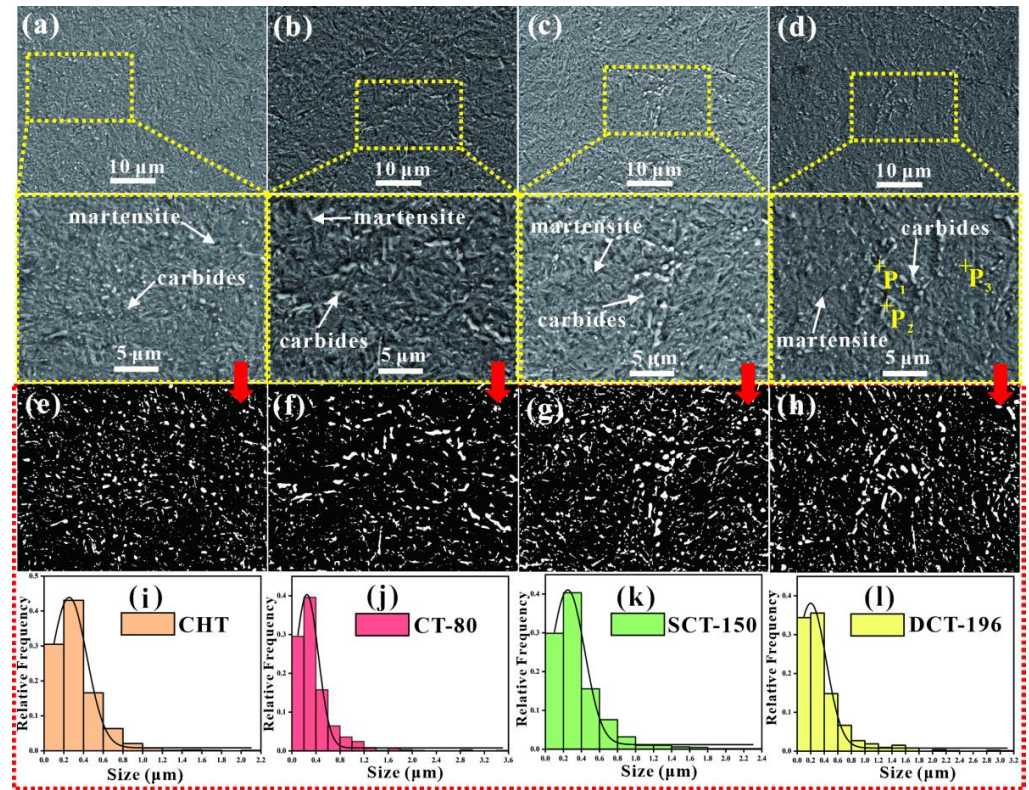


Figure 4. SEM images of the samples at 0.2 mm from the surface: (a) CHT, (b) CT-80, (c) SCT-150, and (d) DCT-196; Pictures after PS processing: (e) CHT, (f) CT-80, (g) SCT-150, and (h) DCT-196; and histogram of carbide calculation results: (i) CHT, (j) CT-80, (k) SCT-150, and (l) DCT-196.

Table 3. EDS results of points P₁, P₂, and P₃.

Sample	Point	at.%						
		C	Ni	Cr	Mn	V	Si	Fe
DCT-196	P1	46.21	0.51	2.68	0.55	-	0.22	49.83
	P2	47.91	0.71	3.85	0.65	0.06	0.24	46.58
	P3	29.60	1.02	1.35	0.25	0.12	0.27	67.37

The SEM microstructure of the core of the sample under different temperatures of cryogenic treatment is shown in Figure 5. As can be seen from Figure 5, the core microstructure of all samples consisted of slatted martensite with carbide. Compared with the CHT samples, the martensite slats of the DCT-196 samples are finer and more nanoscale carbides are dispersed in the martensite slat bundles. The presence of large particles of carbide precipitated on the matrix was also found on CT-80. This phenomenon is attributed to the deflection of carbon atoms and the change in vacancy concentration during the cryogenic process [20,21]. The interstitial carbon atoms and vacancies are transformed into a new grain boundary, and the equilibrium concentration of vacancies is reduced during tempering. During tempering, the vacancy equilibrium concentration rises with temperature, resulting in the addition of new grain boundary to the martensitic structure, leading to the martensite slats refining.

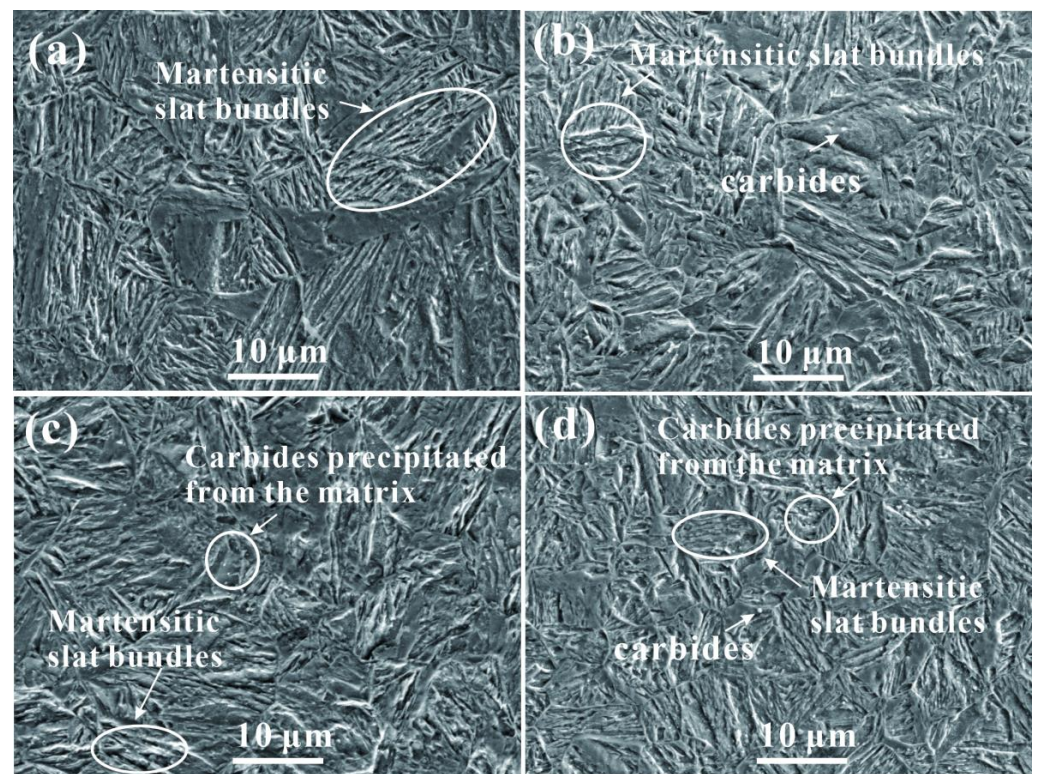


Figure 5. SEM images show the microstructure of the core of (a) CHT, (b) CT-80, (c) SCT-150 and (d) DCT-196 specimens.

The XRD patterns of the samples at a distance of 0.2 mm below the surface subjected to the different treatment taken are presented in Figure 6. From Figure 6a, compared with the standard diffraction patterns of martensite and retained austenite, the diffraction patterns of the retained austenite in the tested samples are shifted towards smaller angles, and that of martensite shifted towards smaller angles then towards bigger angles. With the decrease of the cryogenic treatment temperature, the shifting of diffraction patterns of the retained austenite becomes weaker. The standard diffraction patterns of martensite is 06-0696 with cubic structure $a = 2.8664$, while that of retained austenite is 52-0512 with cubic structure $a = 3.618$. The lattice parameter was calculated by Jade 6.5 software and the results are shown in Table 4. With the decrease of cryogenic treatment temperature, the lattice constant of martensite gradually increased, and the lattice constant of retained austenite remained basically unchanged after decreasing. The fraction of austenite differed for the various samples, and could be calculated from the XRD results using Equation (1) [22].

$$V_{\gamma} = \frac{1.4I_{\gamma}}{I_{\alpha} + 1.4I_{\gamma}} \quad (1)$$

where V_{γ} is the volume fraction of retained austenite, I_{γ} is the mean integrated intensity of the austenite peaks, including the γ (111), γ (200) and γ (220) peaks; and I_{α} is the mean integrated intensity of the martensite peaks, including the M/α (110), M/α (200) and M/α (211) peaks. To reduce the error, the lower angle peaks of γ (111) and M/α (110) were neglected [23]. The calculated retained austenite is 18.15%, 12.92%, 10.37% and 9.45% for the CHT, CT-80, SCT-150 and DCT-196 samples, respectively. From the results, it can be seen that cryogenic treatment can significantly reduce the content of retained austenite, but not eliminate it completely. Cryogenic treatment is not only effective in reducing the retained austenite content; it also affects the shape of the retained austenite. After the cryogenic treatment, the retained austenite will change from massive to thin film [24]. The

film-like austenite distribution in the steel can effectively relieve the stress concentration in the material during service. This improves the toughness of the material [25].

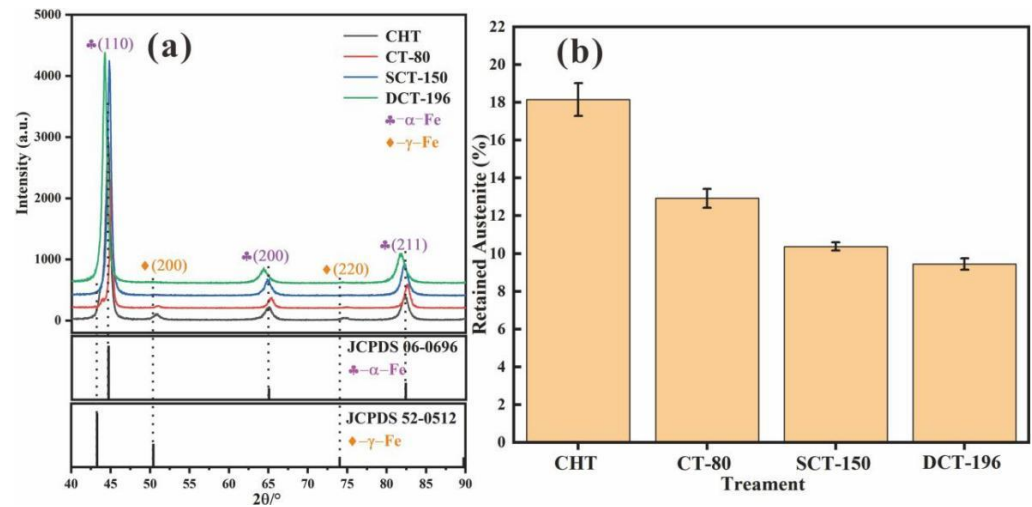


Figure 6. XRD patterns and retained austenite content of 17Cr2Ni2MoVNb steel under different cryogenic treatment processes: (a) XRD patterns, and (b) retained austenite content.

Table 4. The lattice parameters of the phases in 17Cr2Ni2MoVNb steel under different cryogenic treatment processes.

Sample	Phase	Real Lattice Parameter	Standard Lattice Parameter
CH	Martensite	2.8648	2.8664
	Retained austenite	3.6231	3.618
CT-80	Martensite	2.8745	2.8664
	Retained austenite	3.600	3.618
SCT-150	Martensite	2.8803	2.8664
	Retained austenite	3.600	3.618
DCT-196	Martensite	2.8804	2.8664
	Retained austenite	3.601	3.618

3.2. Effect of Cryogenic Treatment on Mechanical Properties

To reveal the effect of the cryogenic treatment on the mechanical properties of alloy steel, the microhardness and wear resistance were measured. Figure 7 shows the microhardness depth profiles of the carburized alloy steel subjected to CHT, CT-80, SCT-150 and DCT-196. Figure 7 clearly shows that the microhardness of the carburized samples subjected to cryogenic treatment was higher near the surface than that of the sample without cryogenic treatment. The carbon concentration on the surface of the specimen is increased after the carburizing process, followed by high temperature tempering and quenching process. At high temperatures, the carbon element undergoes a redox reaction with the oxygen, which leads to a decrease in the carbon concentration on the surface of the sample and forms an internal oxide layer in the carburized layer [26]. There is a small difference between the depth of the hardened layer (at 550 HV) as cryogenic treatment increased the depth of the hardened layer. Owing to the transformation of retained austenite into martensite and the precipitation of carbide in the carburized layer during the cryogenic treatment, the microhardness of the carburized layer is higher than that of the sample without cryogenic treatment. The DCT-196 sample exhibited the highest microhardness. As the cryogenic treatment temperature decreased, the content of retained austenite close to the surface decreased, and the microhardness increased accordingly. However, as the distance increased and the carbon content in the matrix decreased, the content of retained

austenite in the sample decreased, and the change in the hardness became less pronounced, owing to the transformation of retained austenite during the cryogenic treatment.

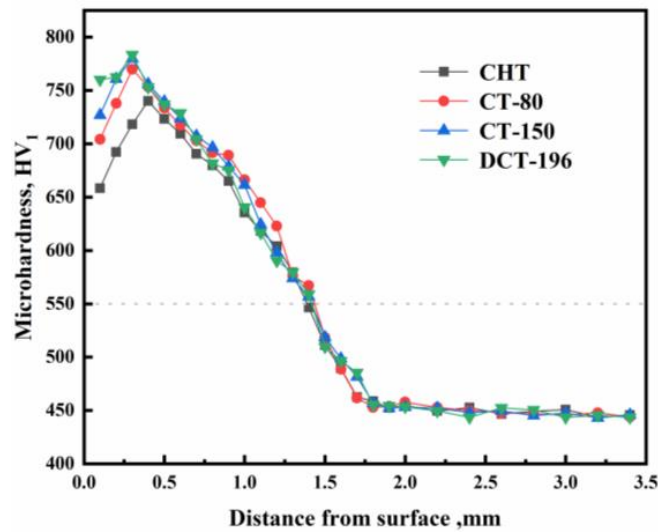


Figure 7. Microhardness of 17Cr2Ni2MoVNb alloys steel under different heat treatments.

Figure 8a shows the relationship between the friction coefficient and time for which 17Cr2Ni2MoVNb steel was subjected to the CHT, CT-80, SCT-150 and DCT-196 processes. At the beginning of the application of friction, the friction coefficients of all the samples increased rapidly. The friction coefficient of the CHT and CT-80 samples increased with time. The friction coefficient of the DCT-196 and SCT-150 samples fluctuated slightly in the first 2 min, and then remained stable at 0.64 and 0.65, respectively. The hardness of the sample is improved due to the reduction of the retained austenite content on the surface after cryogenic treatment. The increase in hardness helps to prevent the frictional substrate from embedding in the substrate and the degree of damage to the substrate is reduced. At the same time, the fine carbides are more uniformly dispersed on the substrate, and the dispersed carbides can effectively impede the dislocation movement of the substrate and increase the wear resistance of the substrate material [27,28].

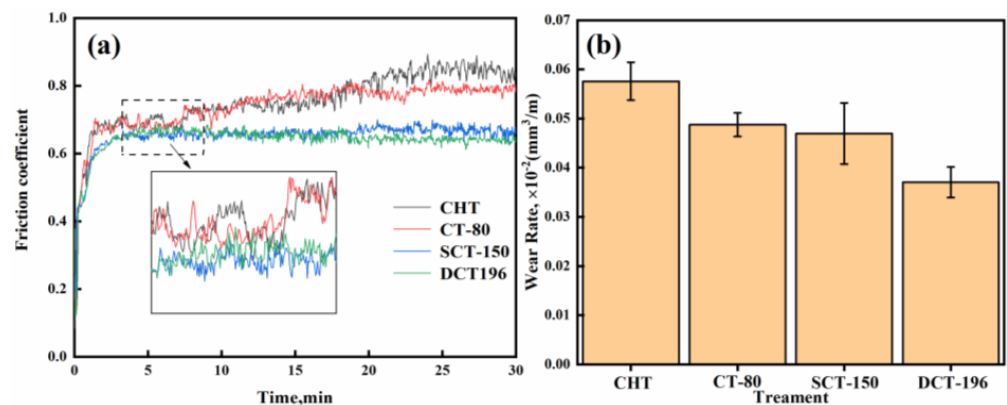


Figure 8. Friction coefficient versus time of 17Cr2Ni2MoVNb alloy steel at different treatment (a) and the wear rate after 30 min (b).

In addition, the depth of the wear scar and the wear volume were tested, subjected to wear for 30 min. The depths of the wear scar were 22.73, 21.85, 19.01 and 18.65 μm for CHT, CT-80, SCT-150 and DCT-196, respectively. The wear volumes were 0.086, 0.073, 0.070 and 0.055 mm^3 for CHT, CT-80, SCT-150 and DCT-196, respectively. The wear rate was calculated to be 0.0576, 0.0487, 0.0470 and 0.0370 $\times 10^{-2} \text{mm}^3/\text{m}$ for CHT, CT-80, SCT-150

and DCT-196 sample, respectively, as shown in Figure 8b and Table 5. The wear resistance of the samples improved after cryogenic treatment. The wear resistance of the carburized steel improved by 15.37%, 18.47% and 35.68% after cryogenic treatment at -80 , -150 and -196 °C, respectively, compared to that of the sample subjected to CHT. The DCT-196 sample had the most stable and lowest friction coefficient, with no significant fluctuation. Here, the wear behaviour of the counterparts to the cryogenic treated samples can be explained by the enhanced amounts of carbides in the latter, which confers good wear resistance compared to the intensive wear experienced by the counterparts. Conversely, this can also be explained by the fact that the matrix of the material has higher hardness, leading to more intensive wear on the counterpart's side.

Table 5. The friction and wear test results of the samples.

Frictional Wear Test Results/Sample	CHT	CT-80	SCT-150	DCT-196
wear scar/ μm	22.73	21.85	19.01	18.65
wear volumes/ mm^3	0.086	0.073	0.070	0.055
wear rate/ $\times 10^{-2} \text{mm}^3/\text{m}$	0.0576	0.0487	0.0470	0.0370
growth rate	0	15.37%	18.47%	35.68%

Figure 9 shows the SEM images of the wear surfaces of the 17Cr2Ni2MoVNb alloy steel subjected to the CHT, CT-80, SCT-150 and DCT-196 processes. The image of the wear surface shows irregular lumpy areas of different contrast and a larger number of grooves parallel to the wear direction. From EDS analysis, the Si and O contents in the dark irregular block areas were 2.09 at.% and 28.01 at.% in the CHT sample, and 1.65 at.% and 26.59 at.% in the CT-80 sample. The change in the friction coefficient and wear morphology is related to the surface state of the alloy steel and the transformation of the wear mechanism. At the initial stage of sliding friction, micro-convex bodies on the alloy steel surface interact first with the opposite Si_3N_4 ball causing a sharp increase in the friction coefficient. As the friction distance increases, some micro-convex bodies are deformed or even worn away. Some of them will remain on the wear surface, resulting in a high level of friction coefficient and the formation of furrows. As more friction is applied, the wear surface of the alloy steel begins to oxidize to form oxide because of the increase in the surface temperature caused by the accumulated frictional heat. It is generally believed that the oxide film formed on the wear surface acts as a solid lubricant with an anti-friction effect. Therefore, the friction coefficient starts to decrease when a certain area of oxide layer is formed on the wear surface. Under the repeated action of frictional force, the oxide film cracks and partially spalls owing to fatigue, after which oxide growth continues in the exposed area [29–31].

The SEM image of the CHT sample shows a larger number of dark irregularities, whereas that of the SCT-150 has a small number of dark irregularities, and the furrows are clearly defined. Crushing and peeling of the oxide layer were clearly seen in the locally enlarged images in Figure 9a,d. Therefore, the friction and wear behaviour of the samples were classified as abrasive wear and oxidation wear.

Combined with the friction coefficient curve in Figure 8a and the wear trace morphology in Figure 7, a correlation between the friction products and the friction coefficient was observed. When the oxidation and spalling processes are in dynamic equilibrium, the friction coefficient remains stable. The friction coefficient should be reduced if the surface hardness increases. The main reasons are as follows: on one hand, the load-bearing capacity and resistance to deformation of the micro-convex bodies are improved, leading to a decrease in the tendency toward adhesion and consequently in the friction coefficient. On the other hand, the stress per unit area increases (the actual contact area decreases), resulting in a higher local temperature and faster oxidation rate [32].

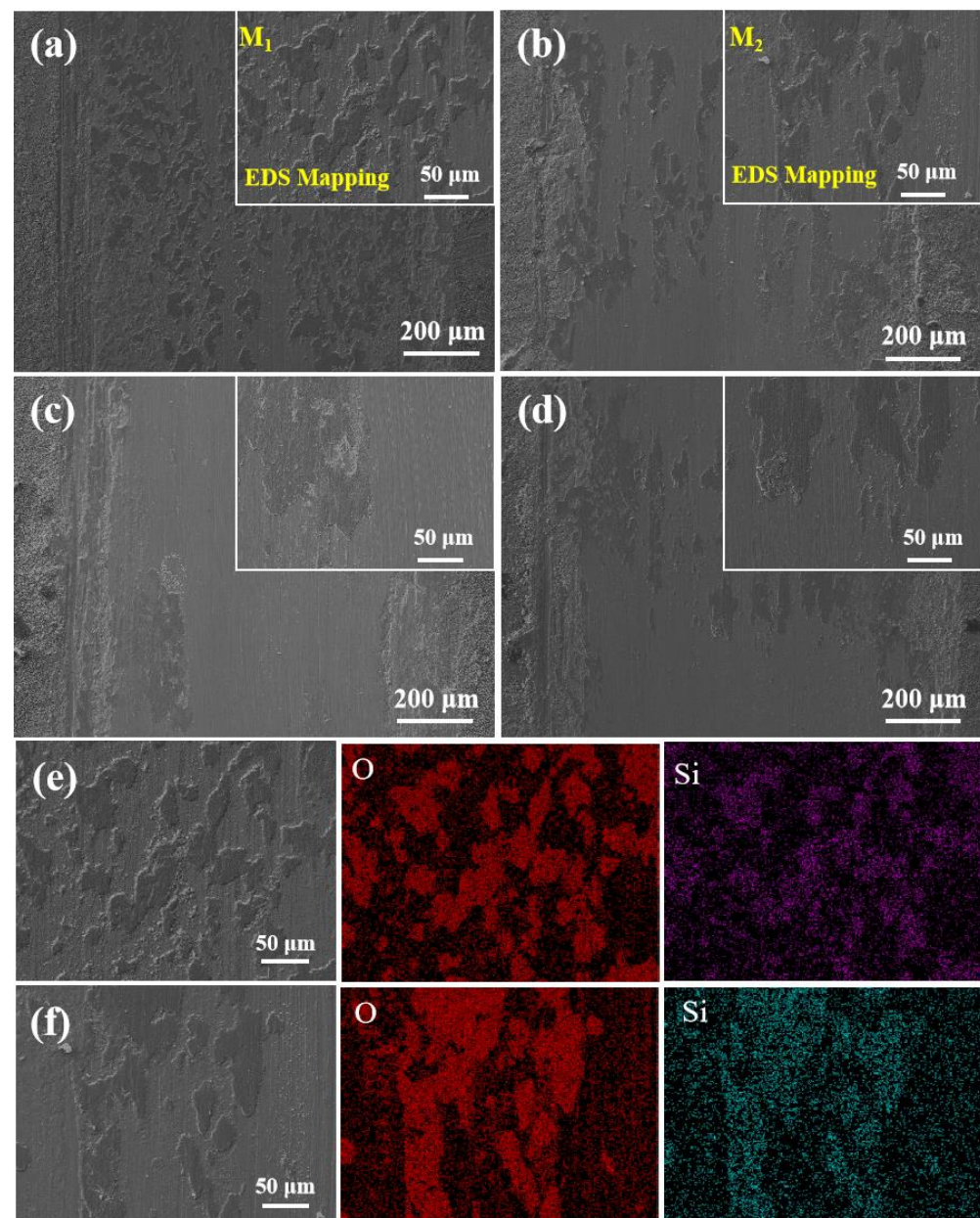


Figure 9. SEM images of the worn-out surfaces of the different samples. (a) CHT, (b) CT-80, (c) SCT-150, and (d) DCT-196. Local magnification of sample with EDS surface scan. (e) CHT, (f) CT-80.

4. Conclusions

The effects of three different temperature (CT-80, SCT-150, DCT-196) cryogenic treatments on the microstructural evolution and mechanical properties of 17Cr2Ni2MoVNb heavy-duty gear steel were investigated. The main conclusions can be drawn as follows:

- (1) When the CHT samples were cryogenic treated at three different temperatures, the retained austenite content was significantly reduced. It is reduced from 18.15% for CHT samples to 12.92% for CT-80, 10.37% for SCT-150 and 9.45% for DCT-196, respectively.
- (2) The cryogenic treatment can increase the degree of carbide precipitation and dispersion. The volume fraction of carbides was calculated to increase from 6.15% in CHT samples to 8.3% in CT-80, 8.7% in SCT-150 and 8.9% in DCT-196, respectively.
- (3) The cryogenic treatment effectively increases the microhardness. The microhardness of each sample increased from 740 HV for CHT samples to 780 HV for CT-80, 780 HV for SCT-150, and 783 HV for DCT-196, respectively.

- (4) The wear resistance of the samples improved after the cryogenic treatment. Compared with sample CHT, the wear resistance of CT-80, SCT-150 and DCT-196 increased to 15.37%, 18.47% and 35.68%, respectively. The main wear mechanisms for the samples were abrasive and oxidative wear.

Author Contributions: Conceptualization, Y.Y.; data curation, Z.L.; funding acquisition: Y.Y. and C.Z.; investigation, Y.Y. and Z.L.; methodology, K.L. and C.Z.; project administration, M.W.; validation, K.L.; writing—original draft, Z.L.; writing—review and editing, Y.Y. and X.W. All authors have read and agreed to the published version of the manuscript.

Funding: This work was supported financially by the National Key Research and Development Program under the Grant No. 20T60860B.

Institutional Review Board Statement: Not applicable.

Informed Consent Statement: Not applicable.

Data Availability Statement: Data sharing is not applicable to this article.

Acknowledgments: The authors gratefully acknowledge the support provided by Fucheng Yin and his team members for X-ray diffraction, metallography and electronic microscopy.

Conflicts of Interest: The authors declare no conflict of interest.

References

- Barron, R.F. Cryogenic treatment of metals to improve wear resistance. *Cryogenics* **1982**, *22*, 409–413. [[CrossRef](#)]
- Zhirafar, S.; Rezaeian, A.; Pugh, M. Effect of cryogenic treatment on the mechanical properties of 4340 steel. *J. Mater. Process. Technol.* **2007**, *186*, 298–303. [[CrossRef](#)]
- SreeramaReddy, T.V.; Sornakumar, T.; VenkataramaReddy, M.; Venkatram, R. Machinability of C45 steel with deep cryogenic treated tungsten carbide cutting tool inserts. *Int. J. Refract. Met. Hard Mater.* **2009**, *27*, 181–185. [[CrossRef](#)]
- Das, D.; Dutta, A.K.; Ray, K.K. Optimization of the duration of cryogenic processing to maximize wear resistance of AISI D2 steel. *Cryogenics* **2009**, *49*, 176–184. [[CrossRef](#)]
- Preciado, M.; Bravo, P.M.; Alegre, J.M. Effect of low temperature tempering prior cryogenic treatment on carburized steels. *J. Mater. Process. Technol.* **2006**, *176*, 41–44. [[CrossRef](#)]
- Çiçek, A.; Kivak, T.; Ekici, E.; Kara, F.; Uçak, N. Performance of Multilayer Coated and Cryo-Treated Uncoated Tools in Machining of AISI H13 Tool Steel—Part 1: Tungsten Carbide End Mills. *J. Mater. Eng. Perform.* **2021**, *30*, 3436–3445. [[CrossRef](#)]
- Gunes, I.; Cicek, A.; Aslantas, K.; Kara, F. Effect of Deep Cryogenic Treatment on Wear Resistance of AISI 52100 Bearing Steel. *Trans. Indian Inst. Met.* **2014**, *67*, 909–917. [[CrossRef](#)]
- Kara, F.; Karabatak, M.; Ayyıldız, M.; Nas, E. Effect of machinability, microstructure and hardness of deep cryogenic treatment in hard turning of AISI D2 steel with ceramic cutting. *J. Mater. Res. Technol.* **2020**, *9*, 969–983. [[CrossRef](#)]
- Kara, F.; Köklü, U.; Kabasakaloğlu, U. Taguchi optimization of surface roughness in grinding of cryogenically treated AISI 5140 steel. *Mater. Test.* **2020**, *62*, 1041–1047. [[CrossRef](#)]
- Qu, S.-G.; Zhang, Y.-L.; Lai, F.-Q.; Li, X.-Q. Effect of Tempering Temperatures on Tensile Properties and Rotary Bending Fatigue Behaviors of 17Cr2Ni2MoVNb Steel. *Metals* **2018**, *8*, 507. [[CrossRef](#)]
- Zhang, Y.; Qu, S.; Lai, F.; Qin, H.; Huang, L.; Li, X. Effect of Quenching Temperature on Microstructure and Rolling Contact Fatigue Behavior of 17Cr2Ni2MoVNb Steel. *Metals* **2018**, *8*, 735. [[CrossRef](#)]
- Da Silva, V.F.; Canale, L.F.; Spinelli, D.; Bose-Filho, W.W.; Crnkovic, O.R. Influence of retained austenite on short fatigue crack growth and wear resistance of case carburized steel. *J. Mater. Eng. Perform.* **1999**, *8*, 543–548. [[CrossRef](#)]
- Delprete, C. Cryogenic treatment: A bibliographic review. *Med. Equip.* **2008**, *13*, 56–57.
- Baldissera, P.; Delprete, C. Effects of deep cryogenic treatment on static mechanical properties of 18NiCrMo5 carburized steel. *Mater. Des.* **2009**, *30*, 1435–1440. [[CrossRef](#)]
- Bensely, A.; Senthilkumar, D.; Lal, D.M.; Nagarajan, G.; Rajadurai, A. Effect of cryogenic treatment on tensile behavior of case carburized steel-815M17. *Mater. Charact.* **2007**, *58*, 485–491. [[CrossRef](#)]
- Bensely, A.; Prabhakaran, A.; Lal, D.M.; Nagarajan, G. Enhancing the wear resistance of case carburized steel (En 353) by cryogenic treatment. *Cryogenics* **2005**, *45*, 747–754. [[CrossRef](#)]
- Jovičević-Klug, P.; Jovičević-Klug, M.; Podgornik, B. Effectiveness of deep cryogenic treatment on carbide precipitation. *J. Mater. Res. Technol.* **2020**, *9*, 13014–13026. [[CrossRef](#)]
- Huang, J.Y.; Zhu, Y.T.; Liao, X.Z.; Beyerlein, I.J.; Bourke, M.A.; Mitchell, T.E. Microstructure of cryogenic treated M2 tool steel. *Mater. Sci. Eng. A* **2003**, *339*, 241–244. [[CrossRef](#)]
- Molinari, A.; Pellizzari, M.; Gialanella, S.; Straffelini, G.; Stiasny, K.H. Effect of deep cryogenic treatment on the mechanical properties of tool steels. *J. Mater. Process. Technol.* **2001**, *118*, 350–355. [[CrossRef](#)]

20. Li, S.; Deng, L.; Wu, X.; Min, Y.a.; Wang, H. Influence of deep cryogenic treatment on microstructure and evaluation by internal friction of a tool steel. *Cryogenics* **2010**, *50*, 754–758. [[CrossRef](#)]
21. Tyshchenko, A.I.; Theisen, W.; Oppenkowski, A.; Siebert, S.; Razumov, O.N.; Skoblik, A.P.; Sirosh, V.A.; Petrov, Y.N.; Gavriljuk, V.G. Low-temperature martensitic transformation and deep cryogenic treatment of a tool steel. *Mater. Sci. Eng. A* **2010**, *527*, 7027–7039. [[CrossRef](#)]
22. Sobotova, J.; Jurci, P.; Dlouhy, I. The effect of subzero treatment on microstructure, fracture toughness, and wear resistance of Vanadis 6 tool steel. *Mater. Sci. Eng. A* **2016**, *652*, 192–204. [[CrossRef](#)]
23. Putra, W.N.; Pramaditya, P.; Pramuka, P.; Ariati, M. Effect of Sub Zero Treatment on Microstructures, Mechanical Properties, and Dimensional Stability of AISI D2 Cold Work Tool Steel. *Mater. Sci. Forum* **2018**, *929*, 136–141. [[CrossRef](#)]
24. Zhang, T.; Hu, J.; Wang, C.; Wang, Y.; Zhang, W.; Di, H.; Xu, W. Effects of deep cryogenic treatment on the microstructure and mechanical properties of an ultrahigh-strength TRIP-aided bainitic steel. *Mater. Charact.* **2021**, *178*, 111247. [[CrossRef](#)]
25. Wang, Y.; Yang, Z.; Zhang, F.; Wu, D. Microstructures and mechanical properties of surface and center of carburizing 23Cr2Ni2Si1Mo steel subjected to low-temperature austempering. *Mater. Sci. Eng. A* **2016**, *670*, 166–177. [[CrossRef](#)]
26. Song, L.; Gu, X.; Sun, F.; Hu, J. Reduced internal oxidation by a rapid carburizing technology enhanced by pre-oxidation for 18CrNiMo7-6 gear steel. *Vacuum* **2019**, *160*, 210–212. [[CrossRef](#)]
27. Gill, S.S.; Singh, J.; Singh, R.; Singh, H. Effect of Cryogenic Treatment on AISI M2 High Speed Steel: Metallurgical and Mechanical Characterization. *J. Mater. Eng. Perform.* **2012**, *21*, 1320–1326. [[CrossRef](#)]
28. Tang, L.; Yan, X.; Jiang, Y.; Li, F.; Zhang, H. Corrigendum to “Effect of Magnetic Field Coupled Deep Cryogenic Treatment on Wear Resistance of AISI 4140 Steel”. *Adv. Mater. Sci. Eng.* **2021**, *2021*, 9837548. [[CrossRef](#)]
29. Hardell, J.; Hernandez, S.; Mozgovoy, S.; Pelcastre, L.; Courbon, C.; Prakash, B. Effect of oxide layers and near surface transformations on friction and wear during tool steel and boron steel interaction at high temperatures. *Wear* **2015**, *330–331*, 223–229. [[CrossRef](#)]
30. Das, D.; Ray, K.K.; Dutta, A.K. Influence of temperature of sub-zero treatments on the wear behaviour of die steel. *Wear* **2009**, *267*, 1361–1370. [[CrossRef](#)]
31. Yan, X.G.; Li, D.Y. Effects of the sub-zero treatment condition on microstructure, mechanical behavior and wear resistance of W9Mo3Cr4V high speed steel. *Wear* **2013**, *302*, 854–862. [[CrossRef](#)]
32. Iakovakis, E.; Roy, M.J.; Gee, M.; Matthews, A. Evaluation of wear mechanisms in additive manufactured carbide-rich tool steels. *Wear* **2020**, *462–463*, 203449. [[CrossRef](#)]